Cardiac Autoantibodies Against Cardiac Troponin I in Post-Myocardial Infarction Heart Failure: Evaluation in a Novel Murine Model and Applications in Therapeutics

古澤, 峻

Cardiac autoantibodies against cardiac troponin I in post-myocardial infarction heart failure: Evaluation in a novel murine model and applications in therapeutics

Shun Furusawa MD[1, 2]; Masataka Ikeda MD, PhD[1, 2]*; Tomomi Ide MD, PhD[1, 2]*; Takuya Kanamura MD[1, 2]; Hiroko Deguchi Miyamoto MD, PhD[1, 2]; Ko Abe MD, PhD[1, 2]; Kosei Ishimaru MD[1, 2]; Masatsugu Watanabe MD[1, 2, 3]; Yoshitomo Tsutsui MD[1, 2]; Ryo Miyake MD[1, 2]; Satoshi Fujita MD[1, 2]; Takeshi Tohyama MD, PhD[1, 4]; Shouji Matsushima MD, PhD[1, 2]; Yoshihiro Baba PhD.[5]; Hiroyuki Tsutsui MD, PhD[1, 2, 6]

[1]Department of Cardiovascular Medicine, Faculty of Medical Sciences, Kyushu University, Fukuoka, Japan

[2]Division of Cardiovascular Medicine, Research Institute of Angiocardiology, Faculty of Medical Sciences, Kyushu University, Fukuoka, Japan

[3]Department of Anesthesiology and Critical Care Medicine, Graduate School of Medical Sciences, Kyushu University, Fukuoka, Japan

[4] Center for Clinical and Translational Research of Kyushu University Hospital, Fukuoka, Japan

[5]Division of Immunology and Genome Biology, Department of Molecular Genetics, Medical Institute of Bioregulation, Kyushu University, Fukuoka, Japan

[6]School of Medicine and Graduate School, International University of Health and Welfare, Fukuoka, Japan

Short title: Cardiac autoantibodies in post-MI heart failure

Correspondence to: Masataka Ikeda, MD, PhD and Tomomi Ide, MD, PhD

Department of Cardiovascular Medicine, Faculty of Medical Sciences, Kyushu University

3-1-1 Maidashi, Higashi-ku, Fukuoka 812-8582, Japan

Phone: +81-92-642-5360; Fax: +81-92-642-5374

Email: ikeda-m@cardiol.med.kyushu-u.ac.jp (M.I.) and tomomi_i@cardiol.med.kyushu-u.ac.jp (T.I.)

Total word count: 3,990 words (Introduction, Methods, Results, Discussion, and Conclusions)

Subject term: Animal Models of Human Disease, Basic Science Research, Pathophysiology, Heart Failure, Inflammatory Heart Disease

Abstract

Background: Cardiac autoantibodies (cAAbs) are involved in the progression of adverse cardiac remodeling in heart failure (HF). However, our understanding of cAAbs in HF is limited owing to the absence of relevant animal models. Herein we aimed to establish and characterize a murine model of cAAb-positive HF after myocardial infarction (MI), thereby facilitating the development of therapeutics targeting cAAbs in post-MI HF.

Methods: MI was induced in BALB/c mice. Plasma cAAbs were evaluated using modified western blot-based methods. Prognosis, cardiac function, inflammation, and fibrosis were compared between cAAb-positive and -negative MI mice. Rapamycin was used to inhibit cAAb production.

Results: Common cAAbs in BALB/c MI mice targeted cardiac troponin I (cTnI). Herein, 71% (24/34) and 44% (12/27) of the male and female MI mice, respectively, were positive for cAAbs against cTnI (cTnIAAb). Germinal centers were formed in the spleens and mediastinal lymph nodes of cTnIAAb-positive MI mice. cTnIAAb-positive MI mice showed progressive cardiac remodeling with a worse prognosis ($p = 0.014$, by

log-rank test), which was accompanied by cardiac inflammation, compared with that in cTnIAAb-negative MI mice. Rapamycin treatment during the first 7 days after MI suppressed cTnIAAb production (cTnIAAb positivity, 59% [29/49] and 7% [2/28] in MI mice treated with vehicle and rapamycin, respectively; $p < 0.001$, by Pearson's χ^2 test), consequently improving the survival and ameliorating cardiac inflammation, cardiac remodeling, and HF in MI mice.

Conclusions: The present post-MI HF model may accelerate our understanding of cTnIAAb and support the development of therapeutics against cTnIAAbs in post-MI HF.

(250/250 words)

Keywords: Cardiac autoantibodies, Heart failure, Myocardial infarction, Troponin I

Clinical Perspective

1) What Is New? (100 words)

- Cardiac autoantibodies (cAAbs) are recognized as pathological features involved in the progression of adverse cardiac remodeling in patients with heart failure (HF);

however, the current understanding of cAAbs is limited.

- We herein developed and characterized a murine HF model with cAAb production against cardiac troponin I after myocardial infarction (MI).
- Our findings revealed the process of cAAb production following MI, its pathological roles in post-MI HF, and a potential therapeutic strategy using rapamycin for suppressing cAAb production following MI.

2) What Are The Clinical Implications? (100 words)

- The number of patients with heart failure (HF) is increasing, and the prognosis of HF remains poor despite medical therapeutic developments with β-blockers and renin-angiotensin system (RAS) inhibitors.
- Our present findings suggest that cardiac autoantibody production against troponin I (cTnIAAb) is a pathological feature and therapeutic target in post-MI HF and that a therapeutic strategy against cAAbs following MI may be clinically feasible.
- The post-MI HF model described herein could accelerate the understanding of cAAb production and facilitate the development of therapeutics for HF, further

improving clinical outcomes following MI.

Non-standard Abbreviations and Acronyms

cAAbs – cardiac autoantibodies; cTnI – cardiac troponin I; cTnIAAb – cardiac autoantibodies against cardiac troponin I; FS – fractional shortening; HF – heart failure; LVEDD – left ventricular end-diastolic diameter; LVEDV – left ventricular end-diastolic volume; LVEF – left ventricular ejection fraction; LVESD – left ventricular end-systolic diameter; LVESV – left ventricular end-systolic volume; MI – myocardial infarction.

Introduction

Heart failure (HF) is a growing public health concern, especially in developed countries.[1] The prevalence of HF is rapidly increasing,[1-3] and an explosive growth in the number of patients with HF is expected in the near future.[4] The mortality rate in patients with HF remains high, although medical and device therapies have improved their clinical outcomes.[5, 6] Thus, it is imperative to further investigate the pathophysiology and develop new therapeutic strategies for HF.

Cardiac autoantibodies (cAAbs) are potential therapeutic targets in HF.[7, 8] Autoantibodies against cardiac troponin I (cTnI) are representative cAAbs observed in patients with ischemic heart disease and dilated cardiomyopathy.[9-13] Approximately 30% of patients with ischemic or dilated cardiomyopathy are positive for autoantibodies against cTnI (cTnIAAbs), although this percentage may vary depending on the positive threshold of the cTnIAAb titer.[14] Notably, the absence of cTnIAAbs may be associated with improvement in cardiac function after acute myocardial infarction (MI).[9] Indeed, several studies have demonstrated that the removal of cAAbs using immunoadsorption offers potential cardioprotection in dilated cardiomyopathy.[15-19] Nevertheless,

immunoadsorption is not a standard therapy for patients with HF because of its temporary therapeutic effect and the difficulty in repeating the therapy. Thus, further research is required to reveal the mechanism underlying cAAb production in HF and to develop therapeutics targeting cAAbs and their production.

Experimental animal models, wherein cAAbs are produced, are limited. Nishimura et al.[20] reported that the deletion of the gene encoding programmed cell death-1 (PD-1) protein spontaneously causes dilated cardiomyopathy along with cAAb production. Okazaki et al.[21] demonstrated that cAAbs in PD-1-deficient mice target cTnI and that the administration of an artificially synthesized antibody that resembles endogenous cTnIAAb in PD-1-deficient mice impairs left ventricular (LV) contractility through the modulation of Ca^{2+} influx in cardiomyocytes. Kaya et al.[22] found that immunization with recombinant cTnI protein could trigger cAAb production in A/J mice, and cAAbs targeting residues 105–122 of murine cTnI are involved in pathological inflammation and fibrosis in the myocardium. Furthermore, cTnIAAb causes spontaneous cardiac inflammation and aggravates the infarct size in MI and ischemia/reperfusion injury.[22-24] However, an animal HF model wherein cAAbs can be observed using the human

disease-mimicking approach is yet to be established. The absence of such a model limits our understanding of cAAbs in HF and hinders the development of cAAb-targeted therapeutics.

In this study, we established and characterized a novel murine model of post-MI HF with cTnIAAbs. Using this model, we investigated the mechanism by which cAAbs are produced after MI and propose potential therapeutic strategies for preventing cAAb production in post-MI HF.

METHODS

A full description of the Materials and Methods can be found in the Supplemental Material. The authors declare that all supporting data are available within the article and Supplemental Material.

Animal experiments

All procedures involving animals and animal care protocols were approved by the Committee on Ethics of Animal Experiments of the Faculty of Medical and

Pharmaceutical Sciences, Kyushu University (A20-049 and A22-008) and performed in accordance with the Guidelines for Animal Experiments of Kyushu University and the Guide for the Care and Use of Laboratory Animals published by the US National Institutes of Health (revised in 2011). The animals were housed in a temperature- and humidity-controlled room, fed a commercial diet (CRF-1; Oriental Yeast Co., Tokyo, Japan), and given free access to water. The murine MI model was established by ligating the left anterior descending (LAD) artery as described previously.[25-27] The details are described in Supplemental Material.

cAAb detection

cAAbs were detected by western blotting as previously described,[20] with slight modifications. Each plasma sample was diluted in 0.5% skim milk (1:500) and loaded onto each lane of the membrane, followed by incubation with the secondary anti-rabbit IgG antibody (1:20,000; #7074; CST) and anti-mouse IgG antibody (1:5000; #7076; CST) diluted in 0.5% skim milk. In the present study, a higher signal intensity of the band probed by plasma cTnIAAb was defined as positivity for cTnIAAb compared with

that observed upon labeling with a specific antibody (ab209809, Abcam [lot #GR298289-2], 2.7 ng/mL [1:50,000]), which was used as the positive control (PC). The details are described in Supplemental Material.

Statistical analysis

All data were statistically analyzed using the JMP16 software (SAS Institute, Cary, NC, USA), and all graphs were plotted using GraphPad Prism version 9.3.1 (GraphPad Software, La Jolla, CA, USA). All data are expressed as mean ± standard deviation (SD). Sample size and power calculations were not conducted before commencing the study, as the present study was exploratory in nature. Statistical significance was determined using the Student's *t*-test, Dunnett's test, and one-way ANOVA followed by post-hoc Tukey's honest significant difference (HSD) test. Pearson's χ^2 and log-rank tests were used for cTnIAAb-positivity percentage and survival analyses, respectively. In the log-rank tests of three groups, post-hoc log-rank analysis for each comparison between two groups were performed only when $p < 0.05$ was confirmed among all groups. To assume the normal distribution of data, the ratiometric data, as indicated in

the figure legends, were log-transformed; the log-transformed data obtained following log_2X data transformation are presented. $p < 0.05$ was considered statistically significant.

RESULTS

cAAb is detected in BALB/c mice after MI

We induced MI in BALB/c mice and found cAAbs, which could bind to cardiac proteins present in murine myocardium lysate, in the plasma of MI mice on day 14 post-MI (Figure 1A). The cAAbs were commonly observed as bands of approximately 25 kDa (Figure 1A), although cAAbs derived from a few MI mice could potentially bind to the other proteins (lanes 3, 6, and 8 in Figure 1A, right). A common band was located at the position corresponding to that of cTnI probed by cTnI-specific antibody. Indeed, all autoantibodies from MI mice reacted with recombinant mouse cTnI (Figure 1B). Moreover, cTnIAAb was identified as the IgG1 isotype (Figure 1C). cAAbs in plasma from an MI mouse (shown in lane #8) reacted with the cardiac antigen derived from rat cardiomyocytes (Figure 1D). Silencing of cTnI in the lysates of rat cardiomyocytes

abolished the corresponding band at 25 kDa (Figure 1E), as observed upon probing using cAAbs (lane #8 plasma in Figure 1D). Collectively, the common cardiac antibodies from post-MI mice were cTnIAAbs.

cTnIAAb binds to cTnI expressed on the cell membrane of cardiomyocytes

To confirm the ability of cTnIAAbs produced in BALB/c MI mice to bind to the outer cell membrane of cardiomyocytes, we first examined the presence of cTnI on the cell membrane using a specific antibody against cTnI (Figure S1A–B) and confirmed that specific antibodies could bind to the outer cell membrane in non-permeabilized cardiomyocytes, using highly sensitive modified immunohistochemistry—the CLAMP method.[28] This binding was attenuated by silencing cTnI, suggesting the presence of membrane-type cTnI. Moreover, cTnIAAb (lane #8 of panel D in Figure 1) could also bind to rat cTnI in non-permeabilized rat cardiomyocytes (Figure 2A, B). Furthermore, the silencing of cTnI reduced the binding of cTnIAAbs to the cell membrane of cultured cardiomyocytes. Collectively, cTnIAAbs can bind to the membrane-type cTnI expressed on cell membranes of cardiomyocytes.

171

172 **Characterization of the post-MI HF model using cTnIAAbs**

173 We next characterized the post-MI murine model for HF with cTnIAAbs. We
174 examined the positivity percentage of cTnIAAb in male and female mice following the
175 experimental protocol shown in Figure S2A. Herein, a higher signal intensity of the
176 band probed by plasma cTnIAAb was defined as positivity for cTnIAAb compared with
177 that observed upon probing by a specific antibody, as described in the Methods (Figure
178 3A). The positivity percentage was significantly higher in male mice than in female
179 mice (71% and 44%, respectively; Figure 3B, $p = 0.039$, analyzed by Pearson's χ^2 test).
180 To further characterize the post-MI HF model with cTnIAAbs, we examined cTnIAAb
181 positivity on days 0, 4, 7, and 14 in the same individual following the experimental
182 protocol shown in Figure S2B. The representative cTnIAAb detection in cTnIAAb-
183 negative (negative #1 and #2) and -positive mice (positive #1 and #2) is shown in
184 Figure 3C. Herein, 8% (2/25) of male and female MI mice were cTnIAAb-positive on
185 day 4 (Figure 3D), and the antibody titer from cTnIAAb-positive mice and the positivity
186 percentage was highest on day 14 after MI (Figure 3D–E). Furthermore, cTnIAAb

positivity continued at least until day 56 (Figure 3E), although its titer was slightly weakened compared with that on day 14. In contrast, no band of cTnIAAb that had a higher signal intensity than the threshold of the positive signal defined in this study was observed in either male or female C57BL/6J mice (0%; n = 10; Figure S3), although weak signals were observed in two male mice (#3 and #7; Figure S3A).

Germinal centers (GCs) were formed in the spleen and mediastinal lymph nodes following MI

GCs are the proliferative grounds for plasma and memory B cells that produce IgGs, which bind efficiently to specific antigens in secondary lymphoid tissues, such as the spleen and lymph nodes.[29] Thus, we examined GC B cells ($CD3^{-}CD19^{+}$) on day 14 post-MI, identified by their high Fas and GL-7 levels in the spleen and mediastinal lymph nodes, by gating as shown in Figure S4A, B. The GC B cells ($CD3^{-}CD19^{+}Fas^{+}GL\text{-}7^{+}$ B cells) number increased significantly in the spleen and mediastinal lymph node of cTnIAAb-positive MI mice, but not in cTnIAAb-negative MI mice (Figure 4A–D). Additionally, the analysis of male and female mice revealed

that GCs were more evident in male mice than in female mice (Figure S4C, D). These results suggest that GCs were likely formed in the spleen and mediastinal lymph nodes, and contained plasma cells that produced high-affinity cTnIAAbs in cTnIAAb-positive MI mice, especially in male mice.

cTnIAAb positivity is associated with adverse cardiac remodeling and poorer prognosis after MI

The percentage of cTnIAAb-positive female mice was 44% and 50%, as shown in Figure 3B and 3D, respectively, whereas that of cTnIAAb-positive male mice was 71% and 67%, as shown in Figure 3B and 3D, respectively. Therefore, we induced MI in female mice to evenly assign MI mice to the cTnIAAb-positive and -negative groups for clarifying the pathological role of cTnIAAb in post-MI HF (Figure S5A–D). Prior to evaluating the survival and cardiac remodeling, we examined the MI-induced myocardial damage in cTnIAAb-positive and -negative mice. No difference in plasma cTnI levels was observed on day 1 after MI between cTnIAAb-positive and -negative mice (Figure 5A; Figure S5A). Furthermore, no difference was observed in the infarct

size of cTnIAAb-positive and -negative mice on day 14 after MI (Figure 5B; Figure S5B). We then evaluated the survival rates of cTnIAAb-positive and -negative mice until day 56 post-MI (Figure S5C). Notably, the prognosis of cTnIAAb-positive MI mice was significantly worse than that of cTnIAAb-negative MI mice (37% *vs*. 76%; hazard ratio: 3.13, confidence interval: 1.21–8.06, $p = 0.014$ by log-rank test; Figure 5C). We further examined cardiac remodeling, represented by LV dilatation and LV ejection fraction (LVEF; Figure S5D). Consistent with the comparable cardiac damages, such as plasma cTnI and infarct size (Figure 5A, B), no differences in echocardiographic parameters, including LVEF and LV end-diastolic diameter (LVEDD), were observed on day 14 post-MI (Table S1). However, LVEF was significantly lower in cTnIAAb-positive mice on day 28 post-MI (Figure 5D). Although a significant difference in average LVEDD on day 28 post-MI was not observed between the two groups (Figure 5D), detailed analysis revealed progressive LV dilatation and contractile dysfunction, represented by ΔLVEF and ΔLVEDD (defined as the difference between days 14 and 28), in cTnIAAb-positive mice, whereas LVEDD and LVEF remained unchanged in cTnIAAb-negative mice until day 28 (Figure 5E;

Figure S5E).

Cardiac inflammation is aggravated in cTnIAAb-positive MI mice

RT-qPCR analysis revealed that the expression of *Il6* and *Ccr2* was upregulated in the myocardium of cTnIAAb-positive MI mice on day 28 (Figure 6A–B). Consistent with the echocardiographic data, *Nppb* expression was elevated in cTnIAAb-positive MI mice (Figure 6C). $CD68^+$ macrophage infiltration and interstitial fibrosis were more pronounced in cTnIAAb-positive MI mice than in cTnIAAb-negative MI mice (Figure 6D, E).

Rapamycin inhibits the production of cTnIAAbs

To prevent cTnIAAb production following MI, we treated male MI mice with rapamycin during the first 7days after MI (Figure S6A–C), since the positivity percentage was higher in male MI mice than in female MI mice (Figure 3B, D). Notably, the positivity percentage was significantly lower in rapamycin-treated MI mice than vehicle-treated mice (7% *vs*. 59%; $p < 0.001$ by Pearson's χ^2 test; Figure 7A).

Rapamycin treatment for 7 days during the initial phase of MI did not change the plasma cTnI levels on day1 after MI (Figure 7B; Figure S6A) and the infarct size on day 14 after MI (Figure 7C; Figure S6B). No differences in echocardiographic parameters, including LVEDD and LVEF, were observed on day 14 post-MI (Table S2, Figure S6C). However, rapamycin treatment improved the survival of post-MI mice compared with that of mice with cTnIAAbs until day 28 post-MI (survival rate: 94%, 65%, and 91% in vehicle-treated cTnIAAb-negative and -positive groups, and rapamycin-treated group, respectively; hazard ratio: 0.23, confidence interval: 0.07–0.79, $p = 0.041$ by log-rank test for rapamycin-treated *vs*. vehicle-treated cTnIAAb-positive groups; Figure 7D) and prevented the progressive cardiac remodeling, as observed in cTnIAAb-positive mice from days 14 to 28 post-MI (Figure 7E, F; Figure S6D). Consistently, *Il6*, *Ccr2*, and *Nppb* expression in rapamycin-treated mice was suppressed compared with that in vehicle-treated cTnIAAb-positive mice (Figure 8A–C). $CD68^+$ macrophages infiltration and interstitial fibrosis were also attenuated in rapamycin-treated MI mice compared with those in vehicle-treated cTnIAAb-positive mice (Figure 8D–E).

DISCUSSION

The immune system and cardiac inflammation can be promising therapeutic targets in HF. Nevertheless, the immunological pathophysiology of HF remains to be fully elucidated, and an effective therapeutic strategy is yet to be established. Here, we report three major findings by developing a murine MI model with cAAbs against cTnI: 1) cAAbs are frequently produced in BALB/c mice, and GCs are formed in the spleen and mediastinal lymph nodes in post-MI BALB/c mice; 2) cAAbs against cTnI are associated with adverse cardiac remodeling, cardiac inflammation, and poor prognosis in post-MI mice; and 3) rapamycin treatment during the initial phase of MI prevent the production of cAAbs, improve the survival, and ameliorate cardiac remodeling and HF, which is accompanied by the suppression of cardiac inflammation, in post-MI mice.

Research on cAAbs in animal models is limited, although previous studies in humans have demonstrated that ~30% of patients with HF are cAAb-positive following MI, which is associated with progressive cardiac dysfunction.[9] Reports from Honjo and colleagues demonstrated that cTnIAAbs were spontaneously produced in PD-1

knockout mice of BALB/c background and administering a monoclonal antibody mimicking endogenous cTnIAAbs in PD-1 mice impaired cardiac contractility.[20, 21] Kaya *et al*.[22, 23] demonstrated that immunization with recombinant cTnI could induce cAAbs against cTnI and lead to cardiac inflammation in A/J mice; moreover, pre-immunization with recombinant cTnI exacerbates the impairment of cardiac function in MI and I/R injury.[24] Nevertheless, an animal cAAb-positive HF model that mimics human disease had not been developed. Here, we developed a human disease-mimicking animal model of HF accompanied by cAAb generation and characterized it by inducing MI in BALB/c mice. Based on previous reports, A/J and BALB/c mice are prospective candidates for developing a cAAb-positive post-MI HF model.[20, 23] We finally decided to induce MI in BALB/c mice because they are more commonly available than A/J mice. Conversely, cAAbs were not evident in C57BL/6J mice, indicating that genetic background is critical for cAAb production following MI. The differences in the genetic background that determine the susceptibility to cAAb production remain unclear, but their recognition may provide important information for identifying high-risk patients who may have cAAbs after MI, especially for the

development of clinically feasible therapeutics targeting cAAbs.

We also observed differences in the positivity of cTnIAAbs, and the likelihood of GCs in the spleen and mediastinal lymph node between male and female mice (Figure 3B, D; Figure S4C, D). Sex-based differences in cAAbs are supported by the weak signals of cTnIAAb only in male and not in female C57BL/6J mice (Figure S3). We initially hypothesized that the amount of cTnI as an antigen in blood was higher in male mice than in female mice, as the heart size was larger in male mice than in female mice. However, no difference in plasma cTnI on day 1 after MI was observed between male and female mice (Figure S7). In general, autoimmune diseases were more common in females than in males, and sex-based difference in autoimmune diseases has been elucidated based on sex chromosomes and hormones such as estrogen and androgen.[30] However, this notion may not be true in cardiac diseases. Given that myocarditis is more common in males than in females,[31, 32] immune responses against the heart may be stronger in males than in females. In this study, we could not reasonably elucidate the sex-based difference in cAAb production, but our observation will be a clue for further investigating the sex-based difference in immune-cardiac diseases.

We identified cTnIAAbs as common cAAbs in the plasma of MI mice. We also observed other protein bands in myocardium lysates (lanes #3, 6, and 8 in Figure 1A), indicating that cAAbs that could bind to other proteins, excluding cTnI, are also produced in BALB/c MI mice. Conversely, cAAbs could bind to recombinant cTnI at different molecular sizes, especially below 25 kDa (Figure 1C), indicating that cTnIAAbs also bind to fragments of recombinant cTnI. Therefore, the band below 25 kDa in lane #8 in Figure 1A may present the degradation of cTnI in the myocardium lysates. Although, in the present study, we focused on the common band representing cTnI, further investigations might be required to clarify the pathological significance of other cAAbs in post-MI HF. In the present study, a positive threshold was prospectively set as the signal intensity probed by a specific primary antibody and a secondary antibody, as described in the Methods, because this signal intensity appeared to be evidently positive for cTnIAAb antibodies. Even so, we also analyzed the relationship between signal intensity and ΔLVEF after collecting all data, retrospectively (Figure S8A). This analysis revealed that the positive threshold defined by the Youden index in the receiver operating characteristic (ROC) curve was 0.71 for predicting the worsening

LVEF from day 14 to 28 in our experiments (Figure S8B, C). Collectively, the positive threshold (= 1) set in this study was approximately equivalent to the Youden index (= 0.71) calculated from echocardiographic data; therefore, it could be validated for underscoring the biological significance of cTnIAAb for adverse cardiac remodeling. However, further investigations are needed to identify the positive threshold of cTnIAAb in humans, which is associated with worsening cardiac remodeling and prognosis in HF.

GCs are likely formed in the spleen and regional mediastinal lymph nodes of cTnIAAb-positive BALB/c mice following MI. However, GCs were also observed in a few cTnIAAb-negative mice (Figure 4). This could be because they were formed in response to cTnI leaked from necrotic myocardial tissue, but myocardial necrosis and subsequent repair were over before high-affinity cTnIAAbs were produced. In this regard, the duration of cTnI leakage from necrotic myocardium during MI might be a critical factor for high-affinity cTnIAAb production. Generally, antibodies steer the protective feedback loop against infection, in which the production of high-affinity Ab must be a trigger for terminating exposure to the antigen by expelling bacteria or

viruses. However, as the cTnI leakage during MI was terminated irrespective of Ab production, incomplete GCs unable to produce high-affinity cTnIAAbs might be formed following MI. Conversely, GCs were not evident in some cTnIAAb-positive MI mice. Collectively, GCs play an important but non-essential role in cTnIAAb production.

The pivotal finding in this study was the evidence that cTnIAAb is associated with cardiac inflammation, progressive cardiac remodeling, and poor prognosis following MI. Nevertheless, the mechanism by which cTnIAAbs impair the myocardium following MI remains debatable. Okazaki *et al.*[21] demonstrated that a monoclonal antibody resembling endogenous cTnIAAb augmented the voltage-dependent L-type Ca^{2+} current of normal cardiomyocytes. Wu *et al.*[33] reported that cTnIAAbs cross-reacted with α-enolase 1 and induced apoptosis in cardiomyocytes. In our model, cleaved caspase-3 representing apoptosis was not pronounced in cTnIAAb-positive mice (Figure S9), although we did not investigate the involvement of Ca^{2+} in cTnIAAb-positive mice. In contrast, we found that the expression of *Il6* and *Ccr2* was upregulated and the number of $CD68^{+}$ macrophages increased in the myocardium of cTnIAAb-positive mice compared with those in cTnIAAb-negative mice, indicating more

363 pronounced inflammation in cTnIAAb-positive mice. We thus deduced that
364 macrophages could bind to the Fc fragment of cTnIAAbs that were bound to
365 cardiomyocytes and these macrophages accumulated in the heart, causing inflammation
366 and impairing the myocardium. However, further investigations are required to clarify
367 the mechanism through which cTnIAAbs promote adverse cardiac remodeling.
368 The human disease-mimicking post-MI HF model with cTnIAAb also enabled the
369 development of therapeutics with rapamycin against cTnIAAb. Rapamycin is an
370 immunosuppressive agent by its action of suppressing inflammatory lymphocytes or
371 activating regulatory T cells (Treg).[34] Rapamycin or rapamycin analogs (rapalogs), such
372 as temsirolimus and everolimus, are used to treat malignancies and for clinical
373 management after organ transplantation.[35, 36] In addition to the clinical application for
374 heart transplantation, rapalogs suppress cardiac hypertrophy[37, 38] and protect the heart
375 from ischemic cardiac injuries, as shown in non-clinical studies.[39, 40] Buss *et al.*[41]
376 demonstrated that treatment with everolimus reduces infarct size and attenuates cardiac
377 remodeling following MI. In fact, high doses of rapamycin (5 mg/kg, once a day,
378 intraperitoneal injection) likely reduced the infarct size in preliminary experiments

(Figure S10). To investigate the effect of cTnIAAbs on adverse cardiac remodeling in MI mice with equal infarct size, we decreased the dose of rapamycin and set the present dose as 3 mg/kg, resulting in comparable infarct size between the rapamycin-treated and -untreated group (Figure 7C). In addition, we limited the therapy duration to the initial 7 days post-MI to minimize the direct effect of rapamycin on cardiac remodeling. Indeed, echocardiographic parameters, such as LVEDD and LVEF, and cardiac damages were comparable between the rapamycin-treated and -untreated groups on day 14 after MI (Figure 7B, C; Table S2), indicating that the present use of rapamycin during the initial phase of MI did not affect cardiac remodeling on day 14 post-MI and that prevention of progressive cardiac remodeling within days 14 and 28 was not relevant to the direct effect of rapamycin on cardiomyocytes. In addition, the protective effect of rapamycin in BALB/c mice was not observed in C57BL/6J mice that did not harbor cAAbs (Figure S11). Moreover, we treated cTnIAAb-negative and -positive MI mice with rapamycin after cTnIAAb production following the protocol shown in Figure S12A and found that rapamycin treatment was ineffective in preventing the progression of adverse cardiac remodeling in cTnIAAb-negative and -positive mice after cTnIAAb production (Figure

S12B–E). Collectively, we reasonably deduced that rapamycin ameliorated cardiac inflammation and adverse cardiac remodeling through the suppression of cAAbs in our experiments. Nevertheless, we acknowledge this issue as a major limitation of the present study because it remains unclear whether the suppressed cTnIAAb production is responsible for the cardioprotective phenotypes under rapamycin treatment.

cTnIAAbs might be a prospective therapeutic target in HF during the early phase of MI. Autoantibodies in autoimmune diseases cannot be fully suppressed by immunosuppressants once their production begins. However, unlike that in other autoimmune diseases, the onset of antibody production in MI is clear as it is accompanied by severe symptoms. Therefore, it is a feasible strategy to prevent cAAb production when MI occurs. Although further investigations are needed to clarify whether rapamycin or rapalogs are the most suitable agents for suppressing cTnIAAb production, the post-MI HF model showing cTnIAAbs established in this study could facilitate the development of therapeutics targeting cTnIAAb production.

Conclusions

We established and characterized a murine model of HF with cTnIAAb production. cTnIAAb was associated with adverse cardiac remodeling and worse prognosis after MI, and rapalogs may be prospective therapeutic agents targeting cTnIAAb production. This new model may support the development of therapeutics targeting cTnIAAb production in patients with post-MI HF.

Acknowledgments

We thank Midori Sato for her technical assistance.

Author Contributions

S Furusawa, MI, TK, HDM, KA, KI, MW, YT, RM, and S Fujita performed the experiments. S Furusawa, MI, TI, TT, SM, and HT interpreted and analyzed data obtained from the experiments. S Furusawa, MI, and TI designed the experimental protocols. S Furusawa, MI, and TI wrote the manuscript and prepared the figures. MI conceived the project. YB critically commented and advised on the project. HT approved and supervised the project. All authors have read and approved the final draft.

Sources of Funding

This work was supported by JSPS KAKENHI (grant numbers JP21K16090 [MI], JP20K08426 [TI], and JP23H02908 [TI]), the Japan Foundation for Applied Enzymology (VBIC: Vascular Biology of Innovation) (MI), MSD Life Science Foundation, the Public Interest Incorporated Foundation (MI), Novartis Pharma Grants for Basic Research 2020 (MI); Kowa Life Science Foundation (MI); SENSHIN Medical Research Foundation (MI); the Cardiovascular Research Fund (Tokyo, Japan) (MI), and the QR program (Qdai-jump Research Program, 02224 [MI]).

Disclosures

Tomomi Ide received research funding from MEDINET, SBI Pharmaceuticals, and Pfizer Japan Co., Ltd. Hiroyuki Tsutsui received remunerations from Daiichi Sankyo, Viatris, Ono Pharmaceutical, Bayer Yakuhin, Otsuka Pharmaceutical, AstraZeneca, Novartis Pharma, and Nippon Boehringer Ingelheim. Research funding was received from MEDINET, Kowa, Nippon Boehringer Ingelheim, Daiichi Sankyo, IQVIA

Services Japan, Johnson & Johnson, NEC Corporation, and Medical Innovation Kyushu. Scholarship funds or donations were received from Otsuka Pharmaceutical, Boston Scientific Japan, Ono Pharmaceutical, Teijin Pharma, Zeon Medical, Bayer Yakuhin, Nippon Boehringer Ingelheim, St. Mary's Hospital, Teijin Home Healthcare, Daiichi Sankyo, Mitsubishi Tanabe Pharma, Abbott Medical Japan, and Japan Lifeline.

Supplemental Material

REFERENCES

1. Virani SS, Alonso A, Benjamin EJ, Bittencourt MS, Callaway CW, Carson AP, Chamberlain AM, Chang AR, Cheng S, Delling FN, et al. Heart disease and stroke statistics-2020 Update: A report from the American Heart Association. *Circulation*. 2020;141:e139–e596.

2. Conrad N, Judge A, Tran J, Mohseni H, Hedgecott D, Crespillo AP, Allison M, Hemingway H, Cleland JG, McMurray JJV, et al. Temporal trends and patterns in heart failure incidence: a population-based study of 4 million individuals. *Lancet*. 2018;391:572–580.

3. Ide T, Kaku H, Matsushima S, Tohyama T, Enzan N, Funakoshi K, Sumita Y, Nakai M, Nishimura K, Miyamoto Y, et al. Clinical characteristics and outcomes of hospitalized patients with heart failure from the large-scale Japanese Registry Of Acute Decompensated Heart Failure (JROADHF). *Circ J*. 2021;85:1438–1450.

4. Heidenreich PA, Albert NM, Allen LA, Bluemke DA, Butler J, Fonarow GC, Ikonomidis JS, Khavjou O, Konstam MA, Maddox TM, et al. Forecasting the impact of heart failure in the United States: a policy statement from the American Heart

Association. *Circ Heart Fail*. 2013;6:606–619.

5. Taylor CJ, Ordóñez-Mena JM, Roalfe AK, Lay-Flurrie S, Jones NR, Marshall T, Hobbs FDR. Trends in survival after a diagnosis of heart failure in the United Kingdom 2000-2017: population based cohort study. *BMJ*. 2019;364:l223.

6. Tohyama T, Ide T, Ikeda M, Kaku H, Enzan N, Matsushima S, Funakoshi K, Kishimoto J, Todaka K, Tsutsui H. Machine learning-based model for predicting 1 year mortality of hospitalized patients with heart failure. *ESC Heart Fail*. 2021;8:4077–4085.

7. Kaya Z, Leib C, Katus HA. Autoantibodies in heart failure and cardiac dysfunction. *Circ Res*. 2012;110:145–158.

8. Düngen HD, Dordevic A, Felix SB, Pieske B, Voors AA, McMurray JJV, Butler J. β_1-adrenoreceptor autoantibodies in heart failure: physiology and therapeutic implications. *Circ Heart Fail*. 2020;13:e006155.

9. Leuschner F, Li J, Göser S, Reinhardt L, Ottl R, Bride P, Zehelein J, Pfitzer G, Remppis A, Giannitsis E, et al. Absence of auto-antibodies against cardiac troponin I predicts improvement of left ventricular function after acute myocardial infarction.

Eur Heart J. 2008;29:1949–1955.

10. Pettersson K, Eriksson S, Wittfooth S, Engström E, Nieminen M, Sinisalo J. Autoantibodies to cardiac troponin associate with higher initial concentrations and longer release of troponin I in acute coronary syndrome patients. *Clin Chem*. 2009;55:938–945.

11. Lindahl B, Venge P, Eggers KM, Gedeborg R, Ristiniemi N, Wittfooth S, Pettersson K. Autoantibodies to cardiac troponin in acute coronary syndromes. *Clin Chim Acta*. 2010;411:1793–1798.

12. Landsberger M, Staudt A, Choudhury S, Trimpert C, Herda LR, Klingel K, Kandolf R, Schultheiss HP, Kroemer HK, Völker U, et al. Potential role of antibodies against cardiac Kv channel-interacting protein 2 in dilated cardiomyopathy. *Am Heart J*. 2008;156:92–99.e2.

13. Miettinen KH, Eriksson S, Magga J, Tuomainen P, Kuusisto J, Vanninen EJ, Turpeinen A, Punnonen KR, Pettersson K, Peuhkurinen KJ. Clinical significance of troponin I efflux and troponin autoantibodies in patients with dilated cardiomyopathy. *J Card Fail*. 2008;14:481–488.

14. O'Donohoe TJ, Ketheesan N, Schrale RG. Anti-troponin antibodies following myocardial infarction. *J Cardiol*. 2017;69:38–45.

15. Felix SB, Staudt A, Dörffel WV, Stangl V, Merkel K, Pohl M, Döcke WD, Morgera S, Neumayer HH, Wernecke KD, et al. Hemodynamic effects of immunoadsorption and subsequent immunoglobulin substitution in dilated cardiomyopathy: three-month results from a randomized study. *J Am Coll Cardiol*. 2000;35:1590–1598.

16. Staudt A, Schäper F, Stangl V, Plagemann A, Böhm M, Merkel K, Wallukat G, Wernecke KD, Stangl K, Baumann G, et al. Immunohistological changes in dilated cardiomyopathy induced by immunoadsorption therapy and subsequent immunoglobulin substitution. *Circulation*. 2001;103:2681–2686.

17. Felix SB, Staudt A, Landsberger M, Grosse Y, Stangl V, Spielhagen T, Wallukat G, Wernecke KD, Baumann G, Stangl K. Removal of cardiodepressant antibodies in dilated cardiomyopathy by immunoadsorption. *J Am Coll Cardiol*. 2002;39:646–652.

18. Müller J, Wallukat G, Dandel M, Bieda H, Brandes K, Spiegelsberger S, Nissen E, Kunze R, Hetzer R. Immunoglobulin adsorption in patients with idiopathic dilated cardiomyopathy. *Circulation*. 2000;101:385–391.

518 19. Schimke I, Müller J, Priem F, Kruse I, Schön B, Stein J, Kunze R, Wallukat G, Hetzer
519 R. Decreased oxidative stress in patients with idiopathic dilated cardiomyopathy one
520 year after immunoglobulin adsorption. *J Am Coll Cardiol*. 2001;38:178–183.
521 20. Nishimura H, Okazaki T, Tanaka Y, Nakatani K, Hara M, Matsumori A, Sasayama S,
522 Mizoguchi A, Hiai H, Minato N, et al. Autoimmune dilated cardiomyopathy in PD-
523 1 receptor-deficient mice. *Science*. 2001;291:319–322.
524 21. Okazaki T, Tanaka Y, Nishio R, Mitsuiye T, Mizoguchi A, Wang J, Ishida M, Hiai H,
525 Matsumori A, Minato N, et al. Autoantibodies against cardiac troponin I are
526 responsible for dilated cardiomyopathy in PD-1-deficient mice. *Nat Med*.
527 2003;9:1477–1483.
528 22. Kaya Z, Göser S, Buss SJ, Leuschner F, Ottl R, Li J, Völkers M, Zittrich S, Pfitzer
529 G, Rose NR, et al. Identification of cardiac troponin I sequence motifs leading to
530 heart failure by induction of myocardial inflammation and fibrosis. *Circulation*.
531 2008;118:2063–2072.
532 23. Göser S, Andrassy M, Buss SJ, Leuschner F, Volz CH, Ottl R, Zittrich S, Blaudeck
533 N, Hardt SE, Pfitzer G, et al. Cardiac troponin I but not cardiac troponin T induces

534 severe autoimmune inflammation in the myocardium. *Circulation*. 2006;114:1693–
535 1702.
536 24. Volz HC, Buss SJ, Li J, Göser S, Andrassy M, Ottl R, Pfitzer G, Katus HA, Kaya Z.
537 Autoimmunity against cardiac troponin I in ischaemia reperfusion injury. *Eur J Heart*
538 *Fail*. 2011;13:1052–1059.
539 25. Inoue T, Ikeda M, Ide T, Fujino T, Matsuo Y, Arai S, Saku K, Sunagawa K. Twinkle
540 overexpression prevents cardiac rupture after myocardial infarction by alleviating
541 impaired mitochondrial biogenesis. *Am J Physiol Heart Circ Physiol*.
542 2016;311:H509–H519.
543 26. Ikeda M, Ide T, Furusawa S, Ishimaru K, Tadokoro T, Miyamoto HD, Ikeda S, Okabe
544 K, Ishikita A, Abe K, et al. Heart rate reduction with ivabradine prevents cardiac
545 rupture after myocardial infarction in mice. *Cardiovasc Drugs Ther*. 2022;36:257–
546 262.
547 27. Ikeda M, Ide T, Tadokoro T, Miyamoto HD, Ikeda S, Okabe K, Ishikita A, Sato M,
548 Abe K, Furusawa S, et al. Excessive hypoxia-inducible factor-1α expression induces
549 cardiac rupture via p53-dependent apoptosis after myocardial infarction. *J Am Heart*

Assoc. 2021;10:e020895.

28. Noguchi K, Shimomura T, Ohuchi Y, Ishiyama M, Shiga M, Mori T, Katayama Y, Ueno Y. β-galactosidase-catalyzed fluorescent reporter labeling of living cells for sensitive detection of cell surface antigens. *Bioconjug Chem*. 2020;31:1740–1744.
29. Victora GD, Nussenzweig MC. Germinal centers. *Annu Rev Immunol*. 2012;30:429–457.
30. Klein SL and Flanagan KL. Sex difference in immune responses. *Nat Rev Immunol*. 2016;16:626–638.
31. Kyto V, Sipila J and Rautava P. The effects of gender and age on occurrence of clinically suspected myocarditis in adulthood. *Heart*. 2013;99:1681–1684.
32. Patone M, Mei XW, Handunnetthi L, Dixon S, Zaccardi F, Shankar-Hari M, Watkinson P, Khunti K, Harnden A, Coupland CAC, Channon KM, Mills NL, Sheikh A and Hippisley-Cox J. Risk of myocarditis after sequential doses of COVID-19 vaccine and SARS-CoV-2 Infection by age and sex. *Circulation*. 2022;146:743–754.
33. Wu Y, Qin YH, Liu Y, Zhu L, Zhao XX, Liu YY, Luo SW, Tang GS, Shen Q. Cardiac troponin I autoantibody induces myocardial dysfunction by PTEN signaling

566 activation. *EBioMedicine*. 2019;47:329–340.

567 34. Thomson AW, Turnquist HR and Raimondi G. Immunoregulatory functions of

568 mTOR inhibition. *Nat Rev Immunol*. 2009;9:324–337.

569 35. Law BK. Rapamycin: an anti-cancer immunosuppressant? *Crit Rev Oncol Hematol*.

570 2005;56:47–60.

571 36. Stallone G, Infante B, Di Lorenzo A, Rascio F, Zaza G, Grandaliano G. mTOR

572 inhibitors effects on regulatory T cells and on dendritic cells. *J Transl Med*.

573 2016;14:152.

574 37. Sadoshima J, Izumo S. Rapamycin selectively inhibits angiotensin II-induced

575 increase in protein synthesis in cardiac myocytes in vitro. Potential role of 70- kD S6

576 kinase in angiotensin II-induced cardiac hypertrophy. *Circ Res*. 1995;77:1040–1052.

577 38. Shioi T, McMullen JR, Tarnavski O, Converso K, Sherwood MC, Manning WJ,

578 Izumo S. Rapamycin attenuates load-induced cardiac hypertrophy in mice.

579 *Circulation*. 2003;107:1664–1670.

580 39. Sciarretta S, Volpe M, Sadoshima J. Mammalian target of rapamycin signaling in

581 cardiac physiology and disease. *Circ Res*. 2014;114:549–564.

582 40. Sciarretta S, Forte M, Frati G, Sadoshima J. The complex network of mTOR
583 signalling in the heart. *Cardiovasc Res*. 2022;118:424–439.
584 41. Buss SJ, Muenz S, Riffel JH, Malekar P, Hagenmueller M, Weiss CS, Bea F,
585 Bekeredjian R, Schinke-Braun M, Izumo S, et al. Beneficial effects of mammalian
586 target of rapamycin inhibition on left ventricular remodeling after myocardial
587 infarction. *J Am Coll Cardiol*. 2009;54:2435–2446.
588 42. Tadokoro T, Ikeda M, Ide T, Deguchi H, Ikeda S, Okabe K, Ishikita A, Matsushima
589 S, Koumura T, Yamada KI, et al. Mitochondria-dependent ferroptosis plays a pivotal
590 role in doxorubicin cardiotoxicity. *JCI Insight*. 2020;5:e132747.
591 43. Deguchi H, Ikeda M, Ide T, Tadokoro T, Ikeda S, Okabe K, Ishikita A, Saku K,
592 Matsushima S, Tsutsui H. Roxadustat markedly reduces myocardial ischemia
593 reperfusion injury in mice. *Circ J*. 2020;84:1028–1033.
594 44. Ikeda M, Ide T, Fujino T, Arai S, Saku K, Kakino T, Tyynismaa H, Yamasaki T,
595 Yamada KI, Kang D, et al. Overexpression of TFAM or twinkle increases mtDNA
596 copy number and facilitates cardioprotection associated with limited mitochondrial
597 oxidative stress. *PLoS One*. 2015;10:e0119687.

598 45. Ikeda M, Ide T, Fujino T, Matsuo Y, Arai S, Saku K, Kakino T, Oga Y, Nishizaki A,
599 Sunagawa K. The Akt-mTOR axis is a pivotal regulator of eccentric hypertrophy
600 during volume overload. *Sci Rep*. 2015;5:15881.
601 46. Miyamoto HD, Ikeda M, Ide T, Tadokoro T, Furusawa S, Abe K, Ishimaru K, Enzan
602 N, Sada M, Yamamoto T, et al. Iron overload via heme degradation in the
603 endoplasmic reticulum triggers ferroptosis in myocardial ischemia-reperfusion injury.
604 *JACC Basic Transl Sci*. 2022;7:800–819.
605 47. Tadokoro T, Ikeda M, Abe K, Ide T, Miyamoto HD, Furusawa S, Ishimaru K,
606 Watanabe M, Ishikita A, Matsushima S, et al. Ethoxyquin is a competent radical-
607 trapping antioxidant for preventing ferroptosis in doxorubicin cardiotoxicity. *J*
608 *Cardiovasc Pharmacol*. 2022;80:690–699.
609 48. Ikeda M, Ide T, Matsushima S, Ikeda S, Okabe K, Ishikita A, Tadokoro T, Sada M,
610 Abe K, Sato M, et al. Immunomodulatory cell therapy using αGalCer-pulsed
611 dendritic cells ameliorates heart failure in a murine dilated cardiomyopathy model.
612 *Circ Heart Fail*. 2022;0:e009366
613 49. Arai S, Ikeda M, Ide T, Matsuo Y, Fujino T, Hirano K, Sunagawa K, Tsutsui H.

614 Functional loss of DHRS7C induces intracellular Ca_2+ overload and myotube
615 enlargement in C2C12 cells via calpain activation. *Am J Physiol Cell Physiol*.
616 2017;312:C29–C39.
617 50. Abe K, Ikeda M, Ide T, Tadokoro T, Miyamoto DH, Furusawa S, Tsutsui Y, Miyake
618 R, Ishimaru K, Watanabe M, et al. Doxorubicin causes ferroptosis and cardiotoxicity
619 by intercalating into mitochondrial DNA and disrupting Alas1-dependent heme
620 synthesis. *Sci Signal*. 2022;15.
621

622 ## Figure legends

623 **Figure 1. Cardiac autoantibody (cAAb) against cardiac troponin I (cTnIAAb) was**
624 **detected in the plasma of BALB/c mice after myocardial infarction (MI). A**, cAAb
625 detection with a screener blotter. Mouse myocardium lysate was electrophoresed as an
626 antigen. Positive control (PC) for cTnI was labeled with a specific antibody against
627 cTnI. cAAb-negative plasma (left panel) and cAAb-positive plasma (right panel) from
628 MI mice. **B**, cTnIAAb detection with a screener blotter. Recombinant mouse cTnI
629 protein was electrophoresed as an antigen. PC for cTnI was labeled with a specific
630 antibody against cTnI. Lanes #1–4 and lanes #5–8 indicate negative and positive
631 autoantibodies, respectively. **C**, Isotype of cTnIAAb. **D**, cAAb detection with a screener
632 blotter. Rat neonatal cardiomyocyte lysate was electrophoresed as an antigen. PC for
633 cTnI (cTnI-PC) was labeled with a specific antibody. Only the cAAb in lane #8 reacted
634 with the antigen derived from rat neonatal cardiomyocytes. **E,** Western blot analysis of
635 lysates from cardiomyocytes, in which cTnI was silenced, using cAAb derived from MI
636 mice (lane #8 in panel **D**).

637

Figure 2. Cardiac autoantibody against cardiac troponin I (cTnIAAb) bound to cTnI expressed on the cell membrane of rat neonatal cardiomyocytes. A, Immunohistochemistry using cTnIAAb that could react with rat cTnI for binding with non-permeabilized rat neonatal cardiomyocytes. Cultured cardiomyocytes were treated with control and specific siRNA against cTnI (*Tnni3*). The scale bar indicates 20 μm. **B**, Quantification of fluorescence intensity (n = 50 in cTnIAAb-negative plasma in cardiomyocytes transfected with siControl, n = 50 in cTnIAAb-positive plasma in cardiomyocytes transfected with siControl, and n = 50 in cTnIAAb-positive plasma in cardiomyocytes transfected with si-Tnni3). Data are presented as the mean ± SD. Statistical significance was determined using one-way ANOVA with a post-hoc Tukey's HSD test.

Figure 3. Characterization of BALB/c mice producing cardiac autoantibody against cardiac troponin I (cTnIAAb) following myocardial infarction (MI). A, Representative western blots showing cTnIAAb-negative and -positive MI BALB/c mice. Positive control (PC) for cTnI was labeled with a specific antibody against cTnI.

654 **B**, The positivity percentages of cTnIAAb-positive mice in male (*n* = 34) and female (*n*
655 = 27) BALB/c mice on day 14 after MI. **C**, The timing of cTnIAAb induction in
656 BALB/c MI mice. The blood was collected from the same animal on days 0, 4, 7, and
657 14 after MI. **D**, Time course of the positivity percentages of cTnIAAb-positive mice in
658 male (*n* = 15) and female (*n* = 10) mice. **E**, Time course of changes in signal intensity
659 labeled by cTnIAAb until day 56 (*n* = 6). The log-transformed data obtained following
660 $\log_2 X$ data transformation are presented. All plasma samples shown in representative
661 images were derived from male MI mice. Data are presented as the mean ± SD.
662 Statistical significance was determined using Dunnett's test (*vs.* day 0).
663

664 **Figure 4. Presence of germinal centers (GCs) in the mediastinal lymph nodes and**
665 **spleens of BALB/c mice on day 14 after myocardial infarction (MI). A**,
666 Representative flow cytometric analysis for GC-forming B cells ($FAS^+GL\text{-}7^+$) in the
667 spleen. **B**, Quantification of GC cells in the spleen shown in panel **A** (sham, *n* = 15
668 [male mice, *n* = 10; female mice, *n* = 5]; cTnIAAb-negative mice, *n* = 12 [male mice, *n*
669 = 7; female mice, *n* = 5]; cTnIAAb-positive mice, *n* = 15 [male mice, *n* = 9; female

mice, n = 6]). The log-transformed data obtained following log_2X data transformation are presented. **C**, Representative flow cytometric analysis for GC-forming B cells ($FAS^+GL\text{-}7^+$) in the mediastinal lymph node. **D**, Quantification of GC cells in the mediastinal lymph node shown in panel **C** (sham mice, n = 9 [male mice, n = 6; female mice, n = 3]; cTnIAAb-negative mice, n = 11 [male mice, n = 6; female mice, n = 5]; cTnIAAb-positive mice, n = 15 [male mice, n = 9; female mice, n = 6]). The log-transformed data obtained following log_2X data transformation are presented. Mediastinal lymph nodes in seven mice could not be collected for analysis. Data are presented as the mean ± SD. Statistical significance was determined using one-way ANOVA with a post-hoc Tukey's HSD test.

Figure 5. Cardiac autoantibody against cardiac troponin I (cTnIAAb) was associated with adverse cardiac remodeling and poorer prognosis after myocardial infarction (MI). A, Plasma cardiac troponin I (cTnI) in cTnIAAb-negative (n = 15) and -positive mice (n = 9) on day 1 after MI. **B**, Infarct size of cTnIAAb-negative (n = 5) and -positive mice (n = 7) on day 14 after MI. Representative images of infarct size (left

686 panel). The scale bar indicates 1 mm. Quantification of infarct size (right panel). **C**, The
687 survival of cTnIAAb-negative and -positive mice. The log-rank test was used for
688 survival analysis. **D**, Left ventricular ejection fraction (LVEF) and left ventricular end-
689 diastolic diameter (LVEDD) in cTnIAAb-negative (n = 13) and -positive (n = 10) MI
690 mice on day 28 after MI. **E**, Changes in LVEF (ΔLVEF) and LVEDD (ΔLVEDD) from
691 days 14 to 28 in cTnIAAb-negative (n = 13) and -positive (n = 10) MI mice. Data are
692 presented as the mean ± SD. Statistical significance was determined using the Student's
693 t-test.
694
695 **Figure 6. Cardiac inflammation was exacerbated in cardiac autoantibody against**
696 **cardiac troponin I (cTnIAAb)-positive mice. A**, *Il6* expression in the myocardium of
697 sham (n = 14), cTnIAAb-negative (n = 13), and cTnIAAb-positive mice (n = 10). **B**, *Ccr2*
698 expression in the myocardium of sham (n = 14), cTnIAAb-negative (n = 13), and
699 cTnIAAb-positive mice (n = 10). **C**, *Nppb* expression in the myocardium of sham (n =
700 14), cTnIAAb-negative (n = 13), and cTnIAAb-positive mice (n = 10). **D**, Representative
701 images of $CD68^+$ macrophage infiltration in the non-infarcted myocardium of cTnIAAb-

negative and -positive mice on day 28 after MI. The scale bar indicates 50 μm. Quantification of $CD68^+$ cells in sham (n = 7), cTnIAAb-negative (n = 7), and cTnIAAb-positive mice (n = 6). **E**, Representative images of Picro-Sirius Red staining. The scale bar indicates 100 μm. Quantification of fibrosis in the non-infarcted myocardium of sham (n = 7), cTnIAAb-negative (n = 7), and cTnIAAb-positive mice (n = 6). The log-transformed data obtained following $\log_2 X$ data transformation are presented in **A**–**C**. Data are presented as the mean ± SD. Statistical significance was determined using one-way ANOVA with a post-hoc Tukey's HSD test.

Figure 7. Rapamycin treatment prevented cardiac autoantibody against cardiac troponin I (cTnIAAb) production after myocardial infarction (MI). A, Positivity percentage of cTnIAAb-positive mice, treated with vehicle (Veh) and rapamycin (Rapa), on day 14 after MI. **B**, Plasma cardiac troponin I (cTnI) in vehicle-treated mice (cTnIAAb-negative mice, n = 7; cTnIAAb-positive mice, n = 8) and rapamycin-treated mice (n = 11) on day 1 after MI. **C**, Infarct size in rapamycin-treated mice on day 14 after MI. Representative images of infarct size (left panel). The scale bar indicates 1 mm.

718 Quantification of infarct size (right panel); cTnI-negative MI mice treated with Veh, *n* =
719 4; cTnI-positive MI mice treated with Veh, *n* = 6; MI mice treated with Rapa, *n* = 6. **D**,
720 The survival of cTnI-negative MI mice treated with Veh, cTnI-positive MI mice treated
721 with Veh, and MI mice treated with Rapa. The log-rank test was used for survival analysis.
722 **E**, Left ventricular ejection fraction (LVEF) and left ventricular end-diastolic diameter
723 (LVEDD) in cTnIAAb-negative (*n* = 15) and -positive (*n* = 15) MI mice treated with Veh
724 and MI mice treated with Rapa (*n* = 20) on day 28 after MI. **F**, Changes in LVEF (ΔLVEF)
725 and LVEDD (ΔLVEDD) from days 14 to 28 in cTnIAAb-negative (*n* = 15) and -positive
726 (*n* = 15) MI mice treated with Veh and MI mice treated with Rapa (*n* = 20). Data are
727 presented as the mean ± SD. Statistical significance was determined using one-way
728 ANOVA with a post-hoc Tukey's HSD test.
729
730 **Figure 8. Rapamycin treatment in the initial phase of myocardial infarction (MI)**
731 **suppressed cardiac inflammation in the late phase of MI. A,** *Il6* expression in the
732 myocardium of cTnIAAb-negative (*n* = 8) and -positive (*n* = 10) MI mice and rapamycin-
733 treated MI mice (*n* = 11). **B,** *Ccr2* expression in the myocardium of cTnIAAb-negative

(*n* = 8) and -positive (*n* = 10) MI mice and rapamycin-treated MI mice (*n* = 11). **C,** *Nppb* expression in the myocardium of cTnIAAb-negative (*n* = 8) and -positive (*n* = 10) MI mice and rapamycin-treated MI mice (*n* = 11). **D**, Representative images of $CD68^+$ macrophage infiltration in the non-infarcted myocardium of cTnIAAb-negative and -positive mice and rapamycin-treated MI mice on day 28 after MI. The scale bar indicates 50 μm. Quantification of $CD68^+$ cells in cTnIAAb-negative (*n* = 7) and cTnIAAb-positive (*n* = 5) MI mice and rapamycin-treated MI mice (*n* = 9). **E**, Representative images of Picro-Sirius Red staining. The scale bar indicates 100 μm. Quantification of fibrosis in the non-infarcted myocardium of cTnIAAb-negative (*n* = 7) and cTnIAAb-positive (*n* = 5) MI mice and rapamycin-treated MI mice (*n* = 9). The log-transformed data obtained following $\log_2 X$ data transformation are presented in **A**–**C**. Data are presented as the mean ± SD. Statistical significance was determined using one-way ANOVA with a post-hoc Tukey's HSD test.

Figure 1

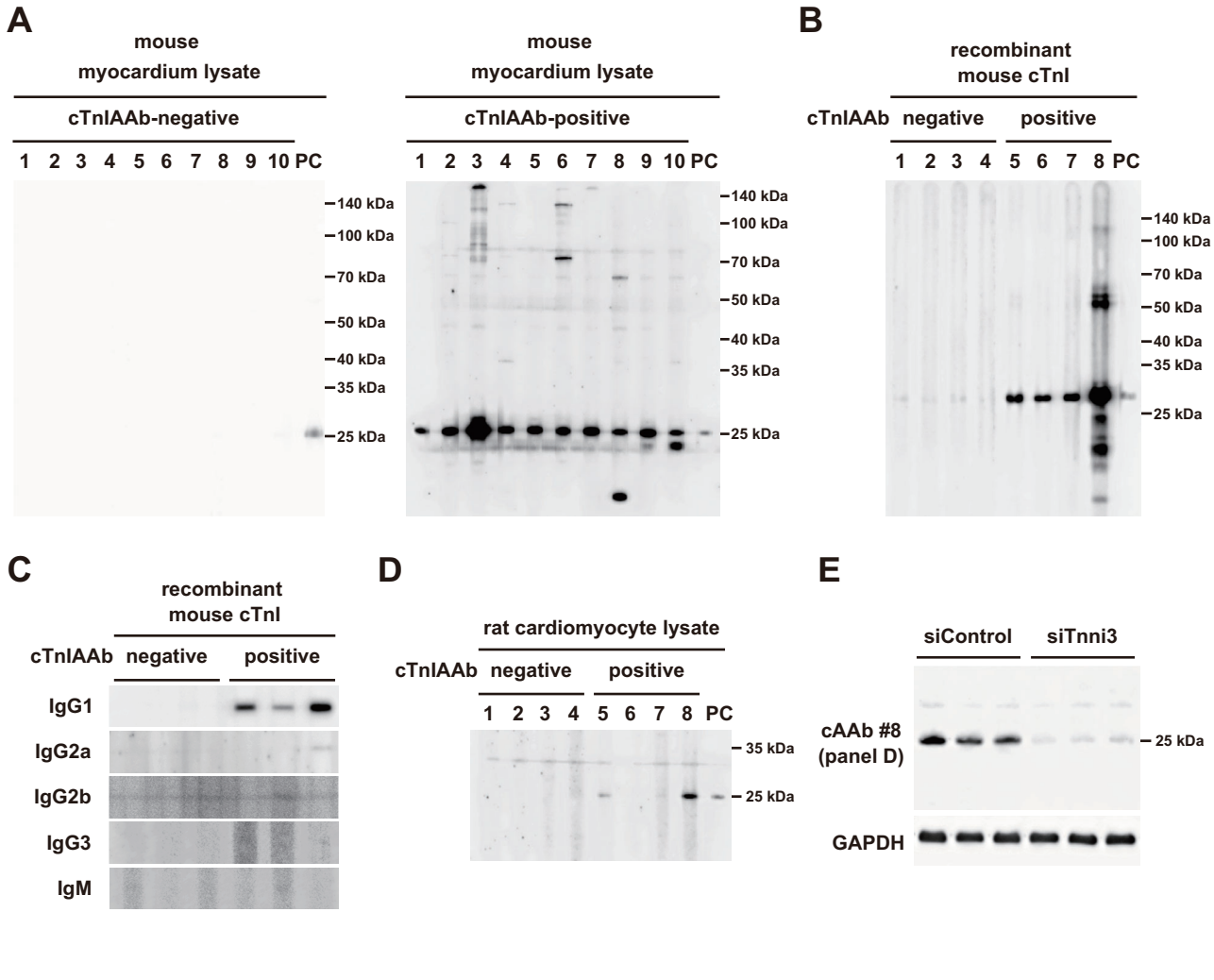
A
mouse
myocardium lysate
cTnIAAb-negative
1 2 3 4 5 6 7 8 9 10 PC
140 kDa
100 kDa
70 kDa
50 kDa
40 kDa
35 kDa
25 kDa
mouse
myocardium lysate
cTnIAAb-positive
1 2 3 4 5 6 7 8 9 10 PC
140 kDa
100 kDa
70 kDa
50 kDa
40 kDa
35 kDa
25 kDa
B
recombinant
mouse cTnI
cTnIAAb negative positive
1 2 3 4 5 6 7 8 PC
140 kDa
100 kDa
70 kDa
50 kDa
40 kDa
35 kDa
25 kDa
C
recombinant
mouse cTnI
cTnIAAb negative positive
IgG1
IgG2a
IgG2b
IgG3
IgM
D
rat cardiomyocyte lysate
cTnIAAb negative positive
1 2 3 4 5 6 7 8 PC
35 kDa
25 kDa
E
siControl
siTnni3
cAAb #8
(panel D)
25 kDa
GAPDH

Figure 2

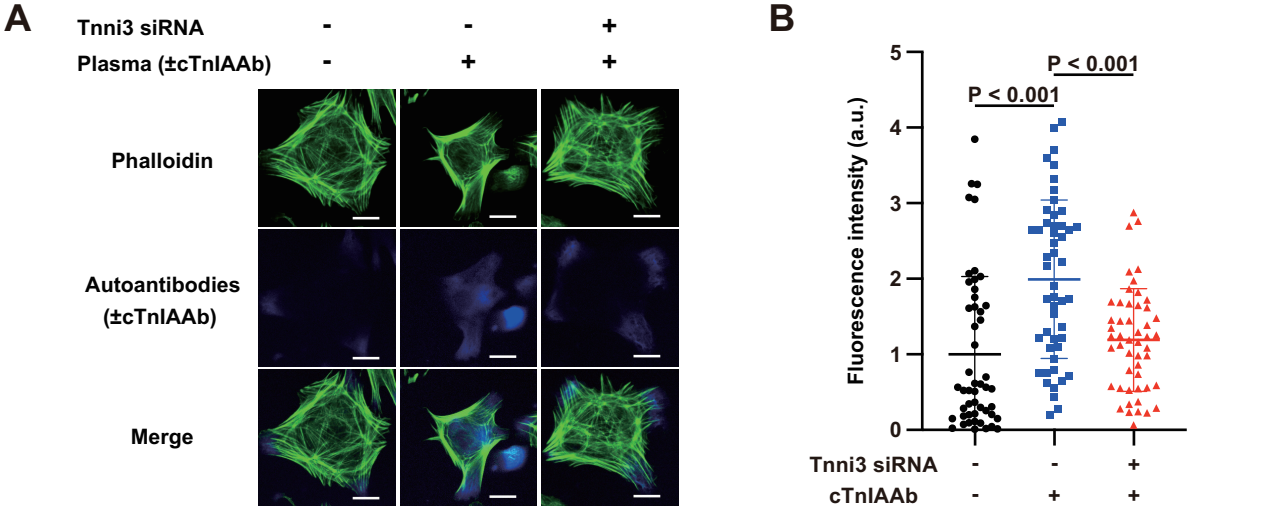
A
Tnni3 siRNA - - +
Plasma (±cTnIAAb) - + +
Phalloidin
Autoantibodies (±cTnIAAb)
Merge
B
Fluorescence intensity (a.u.)
P < 0.001
P < 0.001
0
1
2
3
4
5
Tnni3 siRNA - - +
cTnIAAb - + +

Figure 3

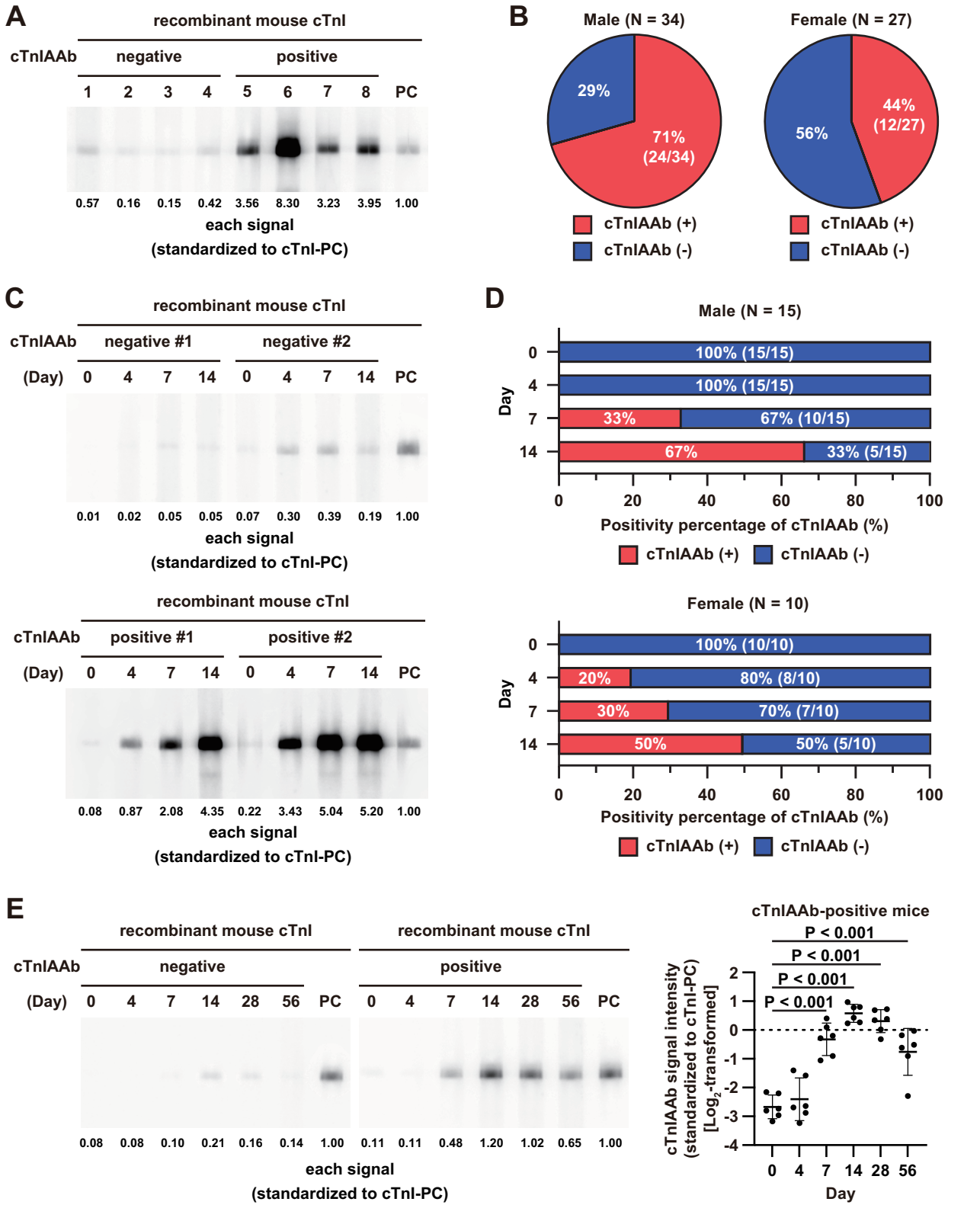
A
recombinant mouse cTnI
cTnIAAb
negative
positive
1 2 3 4 5 6 7 8 PC
0.57 0.16 0.15 0.42 3.56 8.30 3.23 3.95 1.00
each signal
(standardized to cTnI-PC)
B
Male (N = 34)
29%
71%
(24/34)
cTnIAAb (+)
cTnIAAb (-)
Female (N = 27)
56%
44%
(12/27)
cTnIAAb (+)
cTnIAAb (-)
C
recombinant mouse cTnI
cTnIAAb
negative #1
negative #2
(Day) 0 4 7 14 0 4 7 14 PC
0.01 0.02 0.05 0.05 0.07 0.30 0.39 0.19 1.00
each signal
(standardized to cTnI-PC)
recombinant mouse cTnI
cTnIAAb
positive #1
positive #2
(Day) 0 4 7 14 0 4 7 14 PC
0.08 0.87 2.08 4.35 0.22 3.43 5.04 5.20 1.00
each signal
(standardized to cTnI-PC)
D
Male (N = 15)
Day
0 100% (15/15)
4 100% (15/15)
7 33% 67% (10/15)
14 67% 33% (5/15)
0 20 40 60 80 100
Positivity percentage of cTnIAAb (%)
cTnIAAb (+)
cTnIAAb (-)
Female (N = 10)
Day
0 100% (10/10)
4 20% 80% (8/10)
7 30% 70% (7/10)
14 50% 50% (5/10)
0 20 40 60 80 100
Positivity percentage of cTnIAAb (%)
cTnIAAb (+)
cTnIAAb (-)
E
recombinant mouse cTnI
recombinant mouse cTnI
cTnIAAb
negative
positive
(Day) 0 4 7 14 28 56 PC 0 4 7 14 28 56 PC
0.08 0.08 0.10 0.21 0.16 0.14 1.00 0.11 0.11 0.48 1.20 1.02 0.65 1.00
each signal
(standardized to cTnI-PC)
cTnIAAb-positive mice
P < 0.001
P < 0.001
P < 0.001
P < 0.001
cTnIAAb signal intensity
(standardized to cTnI-PC)
[Log2-transformed]
2 1 0 -1 -2 -3 -4
0 4 7 14 28 56
Day

Figure 4

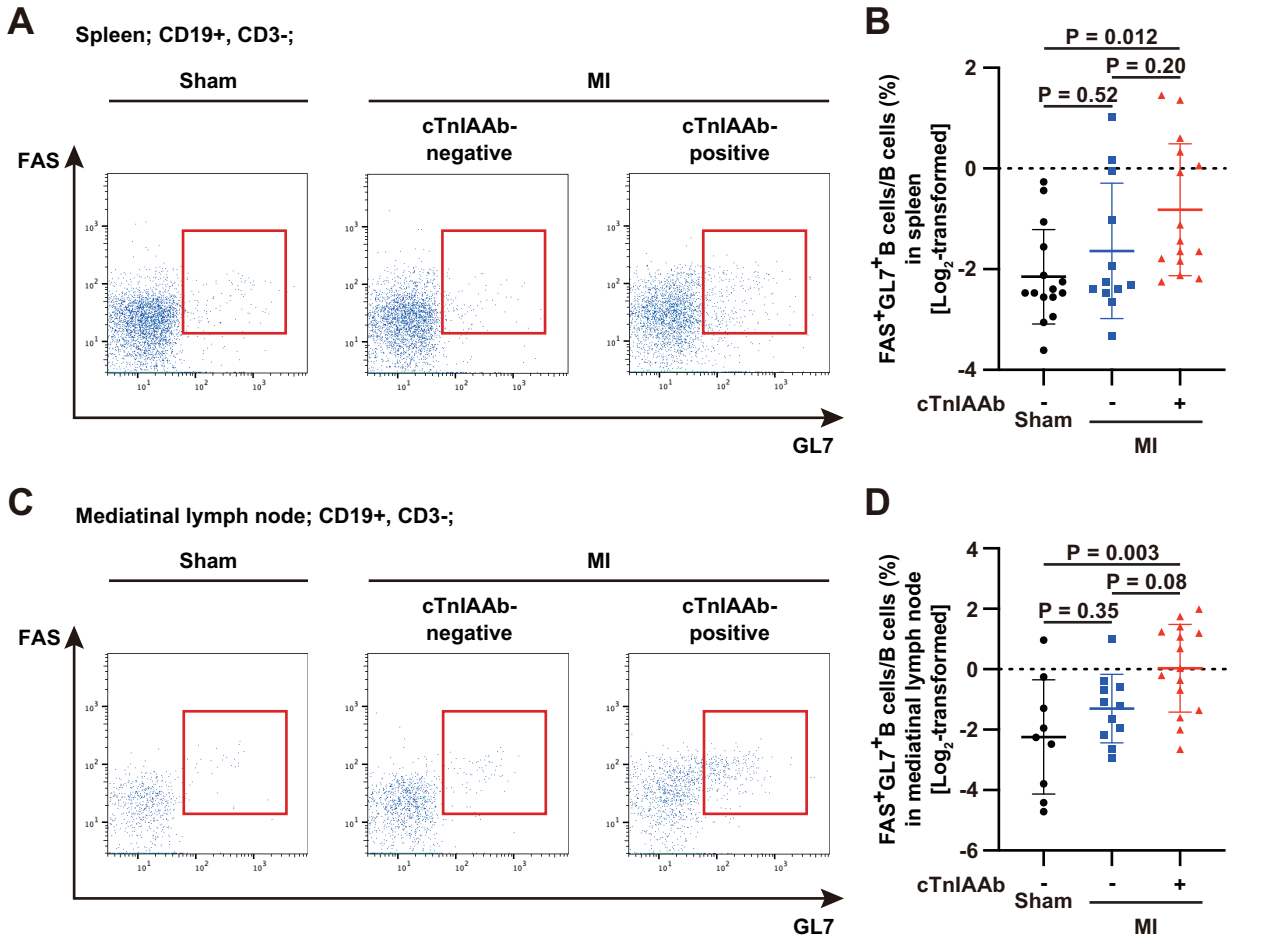
A
Spleen; CD19+, CD3-;
Sham
MI
cTnIAAb-negative
cTnIAAb-positive
FAS
GL7
B
P = 0.012
P = 0.20
P = 0.52
FAS+GL7+B cells/B cells (%) in spleen [Log2-transformed]
cTnIAAb
Sham
MI
C
Mediatinal lymph node; CD19+, CD3-;
Sham
MI
cTnIAAb-negative
cTnIAAb-positive
FAS
GL7
D
P = 0.003
P = 0.08
P = 0.35
FAS+GL7+B cells/B cells (%) in mediatinal lymph node [Log2-transformed]
cTnIAAb
Sham
MI

Figure 5

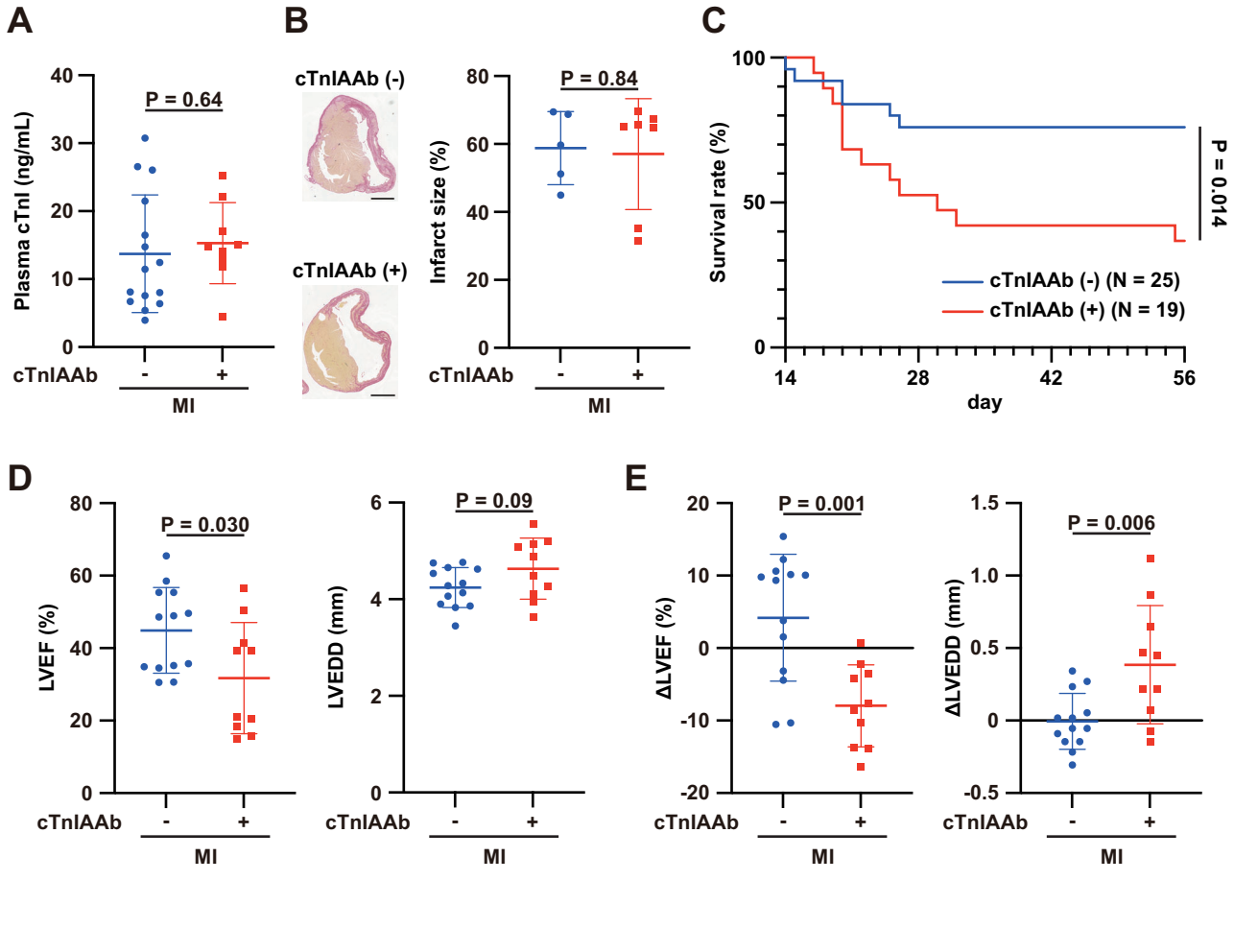
A
Plasma cTnI (ng/mL)
P = 0.64
cTnIAAb
MI
B
cTnIAAb (-)
cTnIAAb (+)
Infarct size (%)
P = 0.84
C
Survival rate (%)
P = 0.014
cTnIAAb (-) (N = 25)
cTnIAAb (+) (N = 19)
day
D
LVEF (%)
P = 0.030
LVEDD (mm)
P = 0.09
E
ΔLVEF (%)
P = 0.001
ΔLVEDD (mm)
P = 0.006

Figure 6

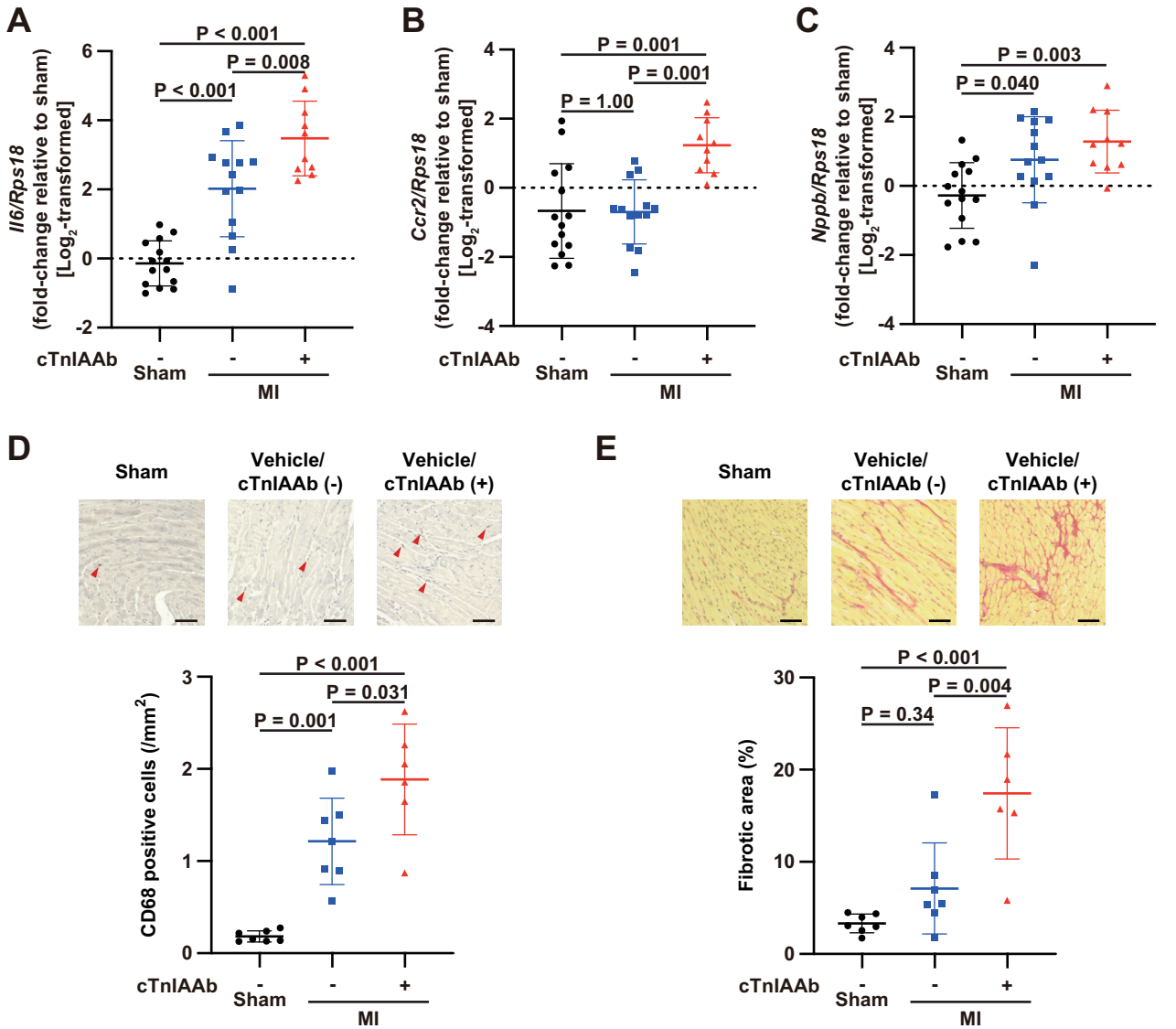
A
Il6/Rps18
(fold-change relative to sham)
[Log2-transformed]
P < 0.001
P = 0.008
P < 0.001
cTnIAAb
Sham
MI
B
Ccr2/Rps18
(fold-change relative to sham)
[Log2-transformed]
P = 0.001
P = 0.001
P = 1.00
cTnIAAb
Sham
MI
C
Nppb/Rps18
(fold-change relative to sham)
[Log2-transformed]
P = 0.003
P = 0.040
cTnIAAb
Sham
MI
D
Sham
Vehicle/
cTnIAAb (-)
Vehicle/
cTnIAAb (+)
CD68 positive cells (/mm2)
P < 0.001
P = 0.031
P = 0.001
cTnIAAb
Sham
MI
E
Sham
Vehicle/
cTnIAAb (-)
Vehicle/
cTnIAAb (+)
Fibrotic area (%)
P < 0.001
P = 0.004
P = 0.34
cTnIAAb
Sham
MI

Figure 7

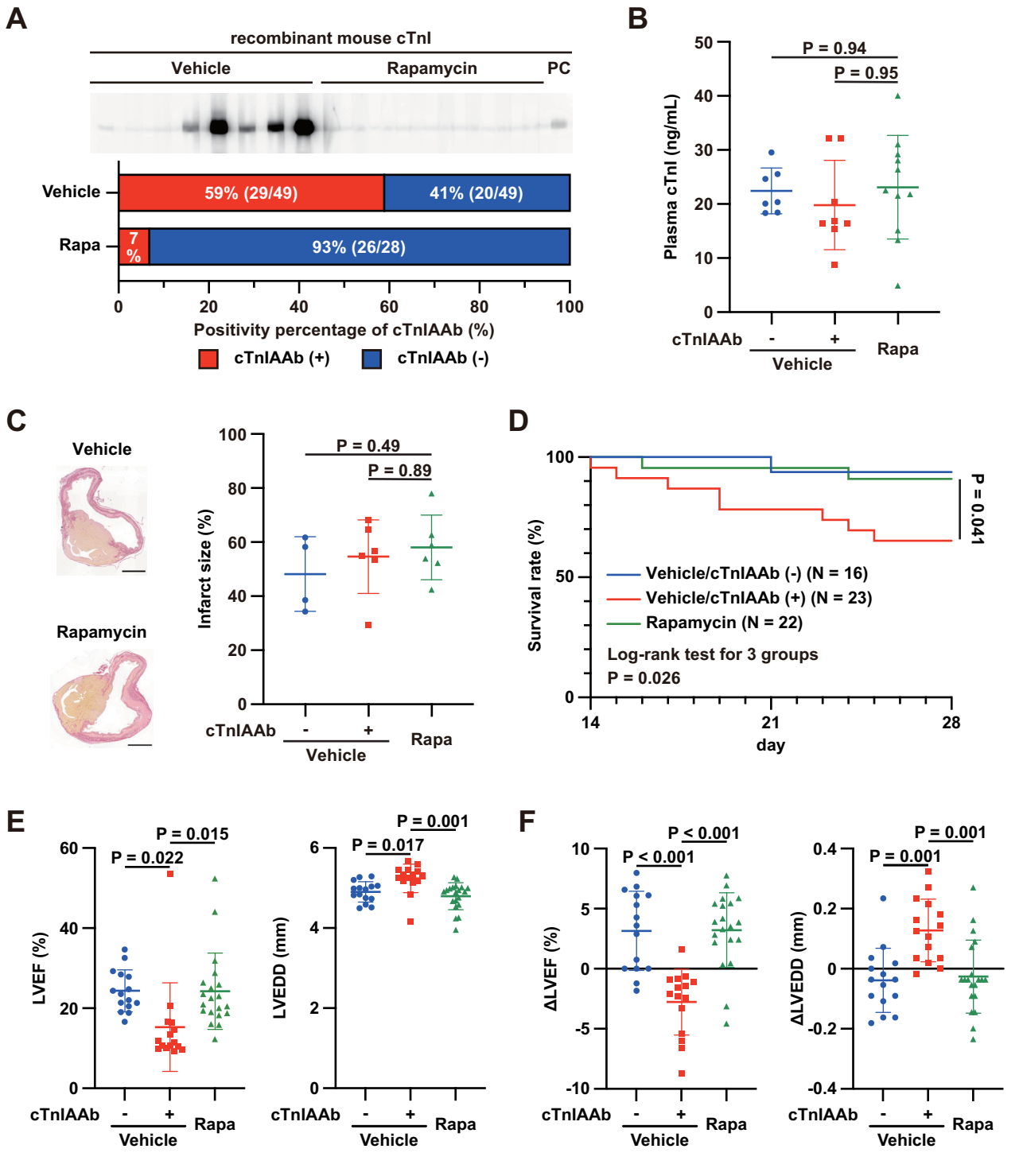
A
recombinant mouse cTnI
Vehicle
Rapamycin
PC
Vehicle
Rapa
59% (29/49)
41% (20/49)
7 %
93% (26/28)
0
20
40
60
80
100
Positivity percentage of cTnIAAb (%)
cTnIAAb (+)
cTnIAAb (-)
B
P = 0.94
P = 0.95
Plasma cTnI (ng/mL)
50
40
30
20
10
0
cTnIAAb
-
+
Vehicle
Rapa
C
Vehicle
Rapamycin
P = 0.49
P = 0.89
Infarct size (%)
100
80
60
40
20
0
cTnIAAb
-
+
Vehicle
Rapa
D
Survival rate (%)
100
50
0
P = 0.041
Vehicle/cTnIAAb (-) (N = 16)
Vehicle/cTnIAAb (+) (N = 23)
Rapamycin (N = 22)
Log-rank test for 3 groups
P = 0.026
14
21
28
day
E
P = 0.015
P = 0.022
LVEF (%)
60
40
20
0
cTnIAAb
-
+
Vehicle
Rapa
P = 0.001
P = 0.017
LVEDD (mm)
6
4
2
0
cTnIAAb
-
+
Vehicle
Rapa
F
P < 0.001
P < 0.001
ΔLVEF (%)
10
5
0
-5
-10
cTnIAAb
-
+
Vehicle
Rapa
P = 0.001
P = 0.001
ΔLVEDD (mm)
0.4
0.2
0
-0.2
-0.4
cTnIAAb
-
+
Vehicle
Rapa

Figure 8

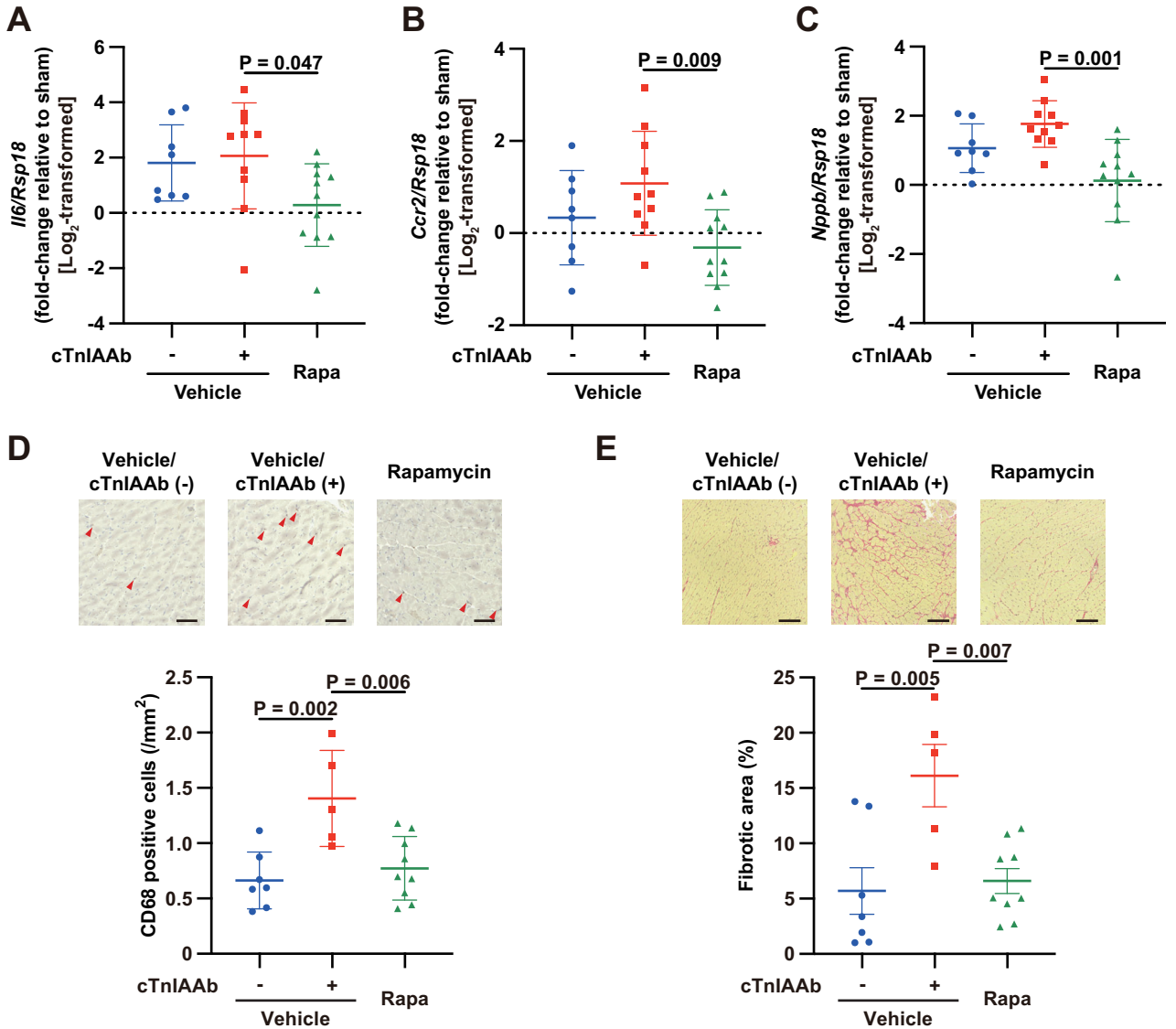
A
Il6/Rsp18
(fold-change relative to sham)
[Log2-transformed]
P = 0.047
cTnIAAb
-
+
Vehicle
Rapa
B
Ccr2/Rsp18
(fold-change relative to sham)
[Log2-transformed]
P = 0.009
cTnIAAb
-
+
Vehicle
Rapa
C
Nppb/Rsp18
(fold-change relative to sham)
[Log2-transformed]
P = 0.001
cTnIAAb
-
+
Vehicle
Rapa
D
Vehicle/
cTnIAAb (-)
Vehicle/
cTnIAAb (+)
Rapamycin
CD68 positive cells (/mm2)
P = 0.006
P = 0.002
cTnIAAb
-
+
Vehicle
Rapa
E
Vehicle/
cTnIAAb (-)
Vehicle/
cTnIAAb (+)
Rapamycin
Fibrotic area (%)
P = 0.007
P = 0.005
cTnIAAb
-
+
Vehicle
Rapa